Research on Chemical Intermediates (2026) 52:631–661
https://doi.org/10.1007/s11164-025-05761-8

New 5-iodoisatin-thiosemicarbazones: preparation, spectroscopic characterization, antioxidant, urease inhibition activities, DFT studies, molecular docking, and molecular dynamic simulations

Hasan Yakan[1] · Halit Muğlu[2] · Temel Kan Bakır[2] · Semiha Yenigün[3] · Amhimmid Ghayth Amhimmid Misbah[2] · Muhammet Serdar Çavuş[4] · Tevfik Özen[3]

Received: 12 June 2025 / Accepted: 20 September 2025 / Published online: 7 October 2025

Abstract

New isatin-thiosemicarbazone compounds (**1**–**7**) were synthesized from numerous thiosemicarbazides and 5-iodoisatin with high yields and efficient methods. The compounds' structures were characterized through FT-IR, ^{1}H NMR, and ^{13}C NMR spectroscopy, supported by elemental analysis. Density functional theory (DFT) calculations were employed to investigate the structural and electronic properties of the compounds, with a discussion on their correlation to antioxidant activity. The antioxidant potential of the synthesized compounds was evaluated in vitro using the 1,1-diphenyl-2-picryl hydrazyl (DPPH·) free radical scavenging assay. These compounds exhibited IC_{50} values ranging from 15.36 ± 0.03 to 22.46 ± 0.05 µM, with compound **7** demonstrating the best antioxidant activity among them. The free radical scavenging effects of the compounds, based on their IC_{50} values, followed the order: **7** > **4** > **6** > **5** > **3** > **2** > **1**. Urease inhibition of the samples and their interactions with urease were examined, and it was determined that compound **2** showed the best inhibition effect and interaction as 1.62 ± 0.05 µg/mL and −7.70 kcal/mol, respectively. Molecular docking was used to ascertain how each molecule interacted with the active areas of the urease enzymes. In addition, molecular dynamics simulation was performed to determine the state of the complex it formed with the enzyme. The current study determined that in vivo biochemical tests of effective thiosemicarbazones could be used to evaluate useful application sectors such as the biological and pharmaceutical fields.

Graphical abstract

New thiosemicarbazone derivatives containing 5-iodoisatin have been synthesized, and their structures have been characterized using various spectroscopic techniques. The antioxidant activity of these compounds was assessed using the DPPH· assay. Additionally, the urease inhibitory effects of the compounds were evaluated, and

Extended author information available on the last page of the article

their interactions with the urease enzyme were studied. Molecular docking studies were conducted to explore how each compound interacts with the active sites of the urease enzyme. Furthermore, molecular dynamics simulations were carried out to investigate the stability and conformation of the enzyme inhibitor complex.

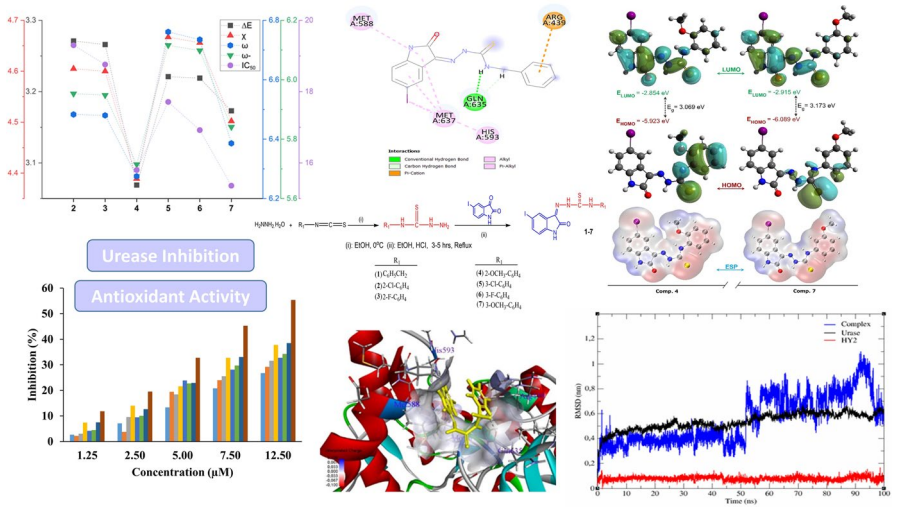

Keywords Thiosemicarbazones · Antioxidant activity · Spectroscopic characterization · Urease inhibition · Molecular docking · DFT

Introduction

Isatins (1H-indole-2,3-diones) represent a significant class of heterocyclic compounds that are present in both plant and human tissues, and these molecules are indole-based derivatives. In the literature, they are known to have many biological and medicinal properties such as antifungal [1, 2], anticancer [3, 4], antibacterial [2], antitubercular [5, 6], enzyme inhibitor [7], antioxidant [8–11], and anti-HIV [2, 12].

Thiosemicarbazones contain the –NH–C(=S)NH–N=linkage and represent a significant class of compounds in synthetic organic chemistry. These molecules act as versatile intermediates, facilitating the synthesis of various structural motifs. Furthermore, they have demonstrated a broad range of biological and medicinal activities, including anticonvulsant [13], anticancer [14–16], enzyme inhibitory activity [17–19], antituberculosis [20], antioxidant agents [21–23], cytotoxicity [24, 25], antitumour [25, 26], antiviral [27], antibacterial [28], and antimicrobial [29].

Antioxidants are gaining a lot of valuation as a global treatment for various lifestyle-related diseases [30]. Cancer, early aging, cardiovascular disease, diabetes, and other degenerative diseases are examples of these illnesses. Reactive oxygen species (ROS) can also induce DNA damage and mutation [31]. Many antioxidant

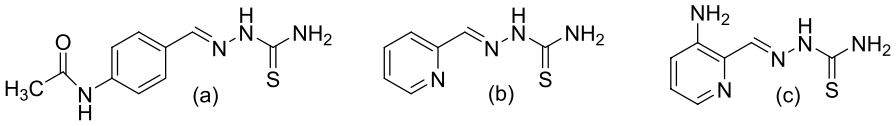

Scheme 1 Structures of thiosemicarbazones used as drugs

compounds and antioxidant enzymes protect against these damages. As a result, various researchers have prepared antioxidant-active chemicals. Numerous eukaryotic and prokaryotic organisms such as bacteria, plants, fungus fungi, algae, and invertebrates have the nickel-containing amidohydrolase urease [31]. Urea is hydrolyzed by urease to produce carbon dioxide and ammonia [32]. It is well known that *Helicobacter pylori* thrives in the stomach when there is an increased ammonia level. High ammonia concentrations caused by urease hyperactivity raise the pH of the stomach and can result in peptic and gastric ulcers, kidney stones, pyelonephritis, and hepatic coma [33–35].

The insertion of synthetic small molecules to decrease urease activity is the most appealing and successful method of controlling its function. This avoids the gastrointestinal issues brought on by hyperactive urease [36]. Few synthetic urease inhibitors have progressed to the next stage of therapeutic research, such as urease inhibitors, despite a few papers on the topic up to this point [37].

Thiosemicarbazones with therapeutic properties, such as *p*-acetylaminobenzaldehyde thiosemicarbazone (Scheme 1a, Thioacetazone®), were used to treat tuberculosis after World War II [38]. The first example of this class of compounds with potent anticancer activity is 2-formylpyridine thiosemicarbazone (Scheme 1b). 3-Amino-pyridine-2-carboxaldehyde thiosemicarbazone (Scheme 1c, 3AP, Triapine®) constitutes one of the most interesting areas of research of thiosemicarbazones for cancer chemotherapy nowadays [39, 40].

In this work, new 5-iodoisatin-thiosemicarbazones were achieved by condensation reaction with 5-iodoisatin and several thiosemicarbazides under reflux in ethanol. The structures of the compounds were elucidated by Fourier transform infrared (FT-IR) and proton–carbon nuclear magnetic resonance (^{1}H–^{13}C NMR) spectroscopic methods and elemental analysis. To our knowledge, the antioxidant and urease inhibitory activities of Schiff bases derived from iodoisatin and thiosemicarbazides are not much in the literature. Therefore, this work seeks to evaluate the antioxidant capacities of several novel thiosemicarbazone molecules. Besides, the compounds' ability to inhibit urease and their interactions with urease were investigated. Especially, the role of substituents on the antioxidant and urease inhibitory properties of the compounds was examined. Each compound's interaction with the urease enzymes' active sites was examined using molecular docking. Moreover, the state of the complex by compound **2**-the enzyme was ascertained by molecular dynamics simulation. Additionally, the spectral and electronic properties of the compounds were analyzed using density functional theory (DFT) calculations. Thiosemicarbazone derivatives, particularly when combined with isatin-based structures, exhibit significant biological activities such as antioxidant and enzyme inhibitory effects. The development of potent antioxidants for the treatment

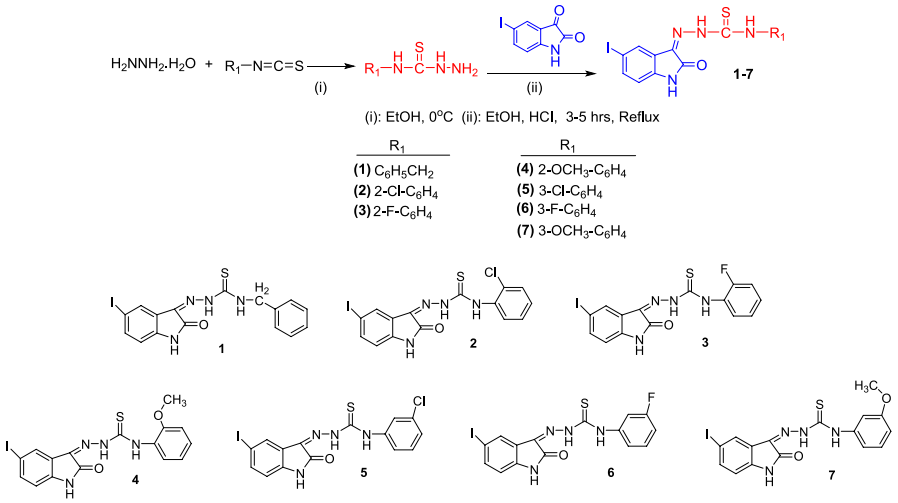

Scheme 2 Molecular structures and synthesis process of new compounds

of oxidative stress-related diseases, along with the discovery of compounds capable of inhibiting biological targets like the urease enzyme, is of great importance for the design of next-generation pharmaceutical agents.

In this context, the newly synthesized isatin-thiosemicarbazone compounds in this study were evaluated for their antioxidant potential and interactions with the urease enzyme. These findings were supported by experimental data, theoretical DFT calculations, and molecular modeling studies. The results indicate that these compounds possess promising potential for biological and pharmaceutical applications.

Experimental

Measurement and reagents

The Supporting Materials contain detailed information.

Synthesis of new compounds (1–7)

The products were obtained using the known procedure, with a few minor modifications [41]. The compounds were efficiently synthesized with yields between 60 and 95%, as illustrated in Scheme 2.

Antioxidant activity measurements

In this experiment, DPPH· scavenging method was performed to investigate free radical scavenging capacities for the produced compounds. This method, which is

accepted in many studies, is based on the principle that compounds acting as hydrogen donors reduce the purple DPPH· solution to a colorless compound [42–45]. In this study, various concentrations (1.25–12.5 µM) were obtained by adding specific volumes of the synthesized compound stock solutions to DPPH· stock solutions, which were prepared in test tubes with ethanol. The compound solutions were prepared by dissolving them in dimethyl sulfoxide (DMSO). Following a 30-min incubation at room temperature, the absorbance was measured at 517 nm. The DPPH· scavenging activity was then determined using the formula [46]:

$$\text{Inhibition } (\%) = \left[\left(A_0 - A_1\right)/A_0\right] \times 100$$

Here, A_0 expresses absorbance of the DPPH· solution without the test compound (control group), and A_1 expresses absorbance of the DPPH· solution with the test compound (experimental group) [47]. Next, the IC_{50} value, commonly used to assess antioxidant activity, was obtained from the equation of the line ($y = mx + c$) derived from the inhibition (%)-concentration curve [48].

Calculation processes

All calculations were performed using the ORCA software [49], employing density functional theory (DFT) [50, 51] for its calculations. The B3LYP functional, combining Becke's three-parameter exchange functional (B3) with the Lee–Yang–Parr correlation functional (LYP), was used along with the def2-QZVP basis set including the D4 dispersion correction. No symmetry restrictions were applied to the compounds during the calculations. TightSCF and TightOpt commands were employed for enhanced accuracy, with automatic generation of the auxiliary basis set via the AutoAux command.

The optimized structures of the compounds correspond to genuine energy minima, as pointed out by the lack of imaginary frequencies in the gas-phase IR calculations.

Electronic parameters were derived from gas-phase calculations at the same level of theory, and these data were then used to determine frontier molecular orbital (FMO) energy eigenvalues. These eigenvalues were subsequently employed to calculate global chemical reactivity parameters, including electronegativity, chemical hardness, and electrophilic index, which provide insights into a molecule's reactivity and stability.

The relative chemical shift values were obtained by subtracting the absolute chemical shielding of tetramethylsilane (TMS), worked out at the B3LYP/def2-QZVP level (31.690 ppm for ^{1}H NMR and 182.473 ppm for ^{13}C NMR), following the re-optimization of the compounds in the DMSO phase and the application of the CPCM-SCRF method for simulating the effects of solvents.

Urease inhibition assay

The indophenol methods revealed the urease inhibitor effects of thiosemicarbazone derivatives [52]. By employing a BIOTEK (Epoch2) microplate reader, the absorbance

values of the blue colors created by the decreasing concentration values of the thiosemicarbazone derivatives including 5-iodoisatin were determined at 630 nm.

Molecule preparation and docking protocol

The geometries of the samples were optimized (energy minimized) using Chem3D 18.0 after being initially drawn in ChemDraw Ultra 18.0. The optimized structures were then converted into Mol2 format. The 3D structure of the enzyme was retrieved from the Protein Data Bank (RCSB PDB), which serves as an information portal for biological macromolecular structures and provides high-quality solutions at various resolutions [53]. The crystal structure of Jack's enzyme, urease, was identified by the PDB ID: 4GY7. Binding affinities were calculated using AutoDock Vina software, and the corresponding binding constants were computed in Excel based on these affinities [54, 55]. Subsequently, the enzyme and the resulting poses were imported into the BIOVIA Discovery Studio 2021 Client program, where both 2D and 3D interaction structures between the target enzyme and the molecules were generated [56, 57].

Molecular dynamic (MD) simulations

The complexes' stability resulting from the docking simulations was assessed through molecular dynamics (MD) modeling. The GROMACS package was used to run MD simulations [58]. The MD simulation made use of the CHARMM force field. The unbound enzyme and its complexes were enclosed in a tricyclic box and solvated using TIP3P water. Na^+ and Cl^- ions were added to the system to neutralize its overall charge. After that, 50.000 steps of the steepest descent technique were used to minimize energy. The system's pressure and temperature were subsequently equilibrated to 100 kPa and 310 K, respectively, using NVT/NPT ensembles. Finally, the MD simulation was executed for 100 ns [59]. To analyze the data of the MD simulation, RMSD (root-mean-square deviation), Rg (radius of gyration), RMSF (root-mean-square fluctuation), and ligand-hydrogen bond plots were generated and evaluated using QtGrace [60–62].

Statistical analysis

The bioactivity results are presented as mean ± standard deviation. Statistical analysis of the entire dataset was carried out using the IBM Statistical Package for the Social Sciences (SPSS) version 20.0. Tukey $HSD^{a,b}$ multiple comparisons were applied to the data, and statistical significance was determined at a p-value of < 0.05.

Results and discussion

Physical properties

Tables 1 and 2 display the data for the physicochemical properties and elemental analyses, respectively.

Vibrational frequencies

In the FT-IR spectra, the stretching bands corresponding to the symmetric and asymmetric vibrations of the amino group (NH_2) were not observed in the range of 3550–3300 cm^{-1}. As a replacement for, new absorptions attributed to the –C=N stretching vibrations of the imine group were observed at 1607–1597 cm^{-1}, indicating a successful reaction as anticipated. For all compounds, the –NH stretching vibrations of the isatin ring appeared between 3358 and 3249 cm^{-1}, while the –NH stretching vibrations of the thiosemicarbazone group were detected in the range of 3224–3141 cm^{-1} (see Support A, Figs. S1–S7). The –C=O stretching vibrations were detected between 1695 and 1682 cm^{-1}, the –C=S signal was observed at 1397–1376 cm^{-1}, the –C–N stretching vibrations appeared between 1309 and 1202 cm^{-1}, and the –C–I stretching vibrations were observed in the range of 568–525 cm^{-1}.

For compounds **2** and **5**, the –C–Cl stretching vibrations were observed at 931 and 956 cm^{-1}, respectively. For compounds **3** and **6**, the –C–F stretching vibrations were detected at 1152 and 1156 cm^{-1}, respectively. For compounds **4** and **7**, the –C–O stretching vibrations were detected at 1148 and 1145 cm^{-1}, respectively.

These spectral features provide strong evidence for the formation of the targeted products, and the experimental and computational IR values of the products are summarized in Table 3. Due to the inability to directly include intermolecular interactions in the calculations, the neglect of anharmonicity, and the effects of the chosen method and basis set, the calculated harmonic vibrational frequencies are generally higher than the observed ones. Therefore, a scaling factor [63] has been applied to the calculated IR values to allow comparison with experimental data, and the values are presented accordingly. These findings are also in agreement with formerly known results for alike compounds. [9, 13, 64].

^{1}H NMR interpretations

For all compounds, the −NH proton signals of the isatin ring were observed as a singlet in the chemical shift range of 11.37–11.30 ppm. The $–N^1H$ and $–N^2H$ proton signals corresponding to the thiosemicarbazone group were detected as singlets at 12.70–12.51 and 10.93–9.92 ppm, respectively (see Support A, Figs. S8–S14). For all compounds, the aromatic proton signals of the phenyl ring (H4–H8) were observed in the range of 7.78–6.86 ppm. In compound **5**, the H4 proton was observed as a singlet at 7.78 ppm. The H6 proton, which coupled with the H7 proton, shown as a doublet at 7.36–7.34 ppm ($J = 7.9$ Hz). The H7 proton, which underwent coupling with both the H6 and H8 protons, displayed a triplet at 7.49–7.45 ppm ($J = 7.9$ Hz), while the H8 proton, which coupled with the H7 proton, was detected as a doublet at 7.65–7.63 ppm ($J = 8.1$ Hz).

In compound **5**, the aromatic proton signals of the isatin ring (H1–H3) were resonated between 8.13 and 6.78 ppm. The H1 proton appeared as a singlet at 8.13 ppm. The H2 proton, which coupled with the H3 proton, was observed as a doublet at

Table 1 Physicochemical properties of the synthesized compounds

Comp.	Structure Name	M. P. (°C)	Yield %	Color
1	*N*-benzyl-2-(5-iodo-2-oxoindolin-3-ylidene)hydrazine-1-carbothioamide	244–246	81	Orange
2	*N*-(2-chlorophenyl)-2-(5-iodo-2-oxoindolin-3-ylidene)hydrazine-1-carbothioamide	272–273	83	Light Orange
3	*N*-(2-fluorophenyl)-2-(5-iodo-2-oxoindolin-3-ylidene)hydrazine-1-carbothioamide	251–252	78	Orange
4	*N*-(2-methoxyphenyl)2-(5-iodo-2-oxoindolin-3-ylidene)hydrazine-1-carbothioamide	259–260	66	Light Brown
5	*N*-(3-chlorophenyl)-2-(5-iodo-2-oxoindolin-3-ylidene)hydrazine-1-carbothioamide	246–247	60	Reddish-brown
6	*N*-(3-fluorophenyl)-2-(5-iodo-2-oxoindolin-3-ylidene)hydrazine-1-carbothioamide	249–250	95	Reddish-brown
7	*N*-(3-methoxyphenyl)-2-(5-iodo-2-oxoindolin-3-ylidene)hydrazine-1-carbothioamide	229–230	75	Orange

Table 2 Elemental analysis results of the compounds

Comp.	Molecular mass (g/mol)	Molecular formula	Calculated			Experimental		
			C%	H%	N%	(C)%	(H)%	(N)%
1	436.0	$C_{16}H_{13}IN_4OS$	44.05	3.00	12.84	43.96	2.95	12.78
2	456.5	$C_{15}H_{10}ClIN_4OS$	39.45	2.21	12.27	39.32	2.26	12.21
3	440.0	$C_{15}H_{10}FIN_4OS$	40.92	2.29	12.73	40.85	2.31	12.67
4	452.0	$C_{16}H_{13}IN_4O_2S$	42.49	2.90	12.39	42.40	2.94	12.42
5	456.5	$C_{15}H_{10}ClIN_4OS$	39.45	2.21	12.27	39.37	2.29	12.25
6	440.0	$C_{15}H_{10}FIN_4OS$	40.92	2.29	12.73	40.84	2.22	12.70
7	452.0	$C_{16}H_{13}IN_4O_2S$	42.49	2.90	12.39	42.57	2.94	12.32

7.69–7.67 ppm ($J = 8.1$ Hz), while the H3 proton, which coupled with the H2 proton, exhibited a doublet at 6.80–6.78 ppm ($J = 8.2$ Hz). For compounds **4** and **7**, the proton signals of methoxy ($–OCH_3$) were observed as a singlet at 3.83 and 3.79 ppm, respectively. For compound **1**, the $–N^2H$ proton signal coupled to the methylene group ($–CH_2–N$) and appeared as a triplet 9.95–9.92 (1H, t, $J = 6.0$ Hz). Similarly, the methylene group ($–CH_2–N$) coupled to $–N^2H$ proton signal and showed as a doublet at 4.90–4.88 (2H, d, $J = 6.0$ Hz) ppm. These findings are in agreement with values reported for alike compounds in the literature [12, 21, 65, 66]. The ^{1}H NMR spectra of all compounds were recorded in DMSO-d_6, and the experimental-calculated chemical shifts are provided in Table 4. The signals corresponding to DMSO-d_6 and water in DMSO (HOD, H_2O) were observed around 2.00, 2.50 (quintet), and 3.40 (variable) ppm, respectively [67].

^{13}C NMR interpretations

The ^{13}C NMR spectra of the compounds were recorded in DMSO-d_6, and the experimental-theoretical chemical shifts are summarized in Table 5. For all compounds (**1–7**), the characteristic –C=O (C7) peaks of the isatin ring were observed in the range of 163.3–162.5 ppm, while the imine (–C=N, C8) signals appeared between 142.6 and 142.3 ppm. Additionally, the notable –C=S (C9) signals of the thiosemicarbazone group were detected between 178.5 and 176.6 ppm (see Support A, Figs. S15–S21). In the compounds (**1–7**), the aromatic carbon signals of the isatin ring (C1–C6) were observed between 139.9 and 85.7 ppm, while the carbon signals from the phenyl ring (C10–C15) were detected in the range of 159.1–111.8 ppm.

In compounds **4** and **7**, the methoxy ($–OCH_3$) carbon atoms were resonated at 56.2 and 55.7 ppm, respectively. In compound **1**, the methylene ($–CH_2$) carbon atom was observed at 47.7 ppm. Additionally, for compounds **3** and **6**, the carbon atoms (C10–C15) from the phenyl ring were split into doublets due to coupling with the fluorine (F) nucleus.

Moreover, in compounds **1–7**, the carbon signals exhibited a downfield shift (higher δ values) compared to the benzene reference signal at 128.5 ppm. This shift is attributed to the electron-withdrawing effects of substituent groups, such as

Table 3 Experimental and calculated IR vibration frequencies of the compounds

	Comp.	ν_{NH} (ist)	ν_{NH} (tcrb)	$\nu_{C=O}$ (ist)	$\nu_{C=N}$	$\nu_{C=S}$	$\nu_{S=C-N}$ ν_{ArC-N}	ν_{C-I}	Subs.
Experimental	**1**	3358	3201	1695	1604	1394	1299, 1243	568	–
	2	3287	3218	1687	1597	1397	1305, 1202	538	C–Cl: 931
	3	3328	3221	1682	1607	1381	1305, 1202	525	C–F: 1152
	4	3285	3224	1687	1606	1376	1309, 1214	534	C–O: 1148
	5	3249	3187	1686	1601	1395	1304, 1203	544	C–Cl: 956
	6	3333	3166	1687	1605	1387	1304, 1261	535	C–F: 1156
	7	3300	3141	1682	1601	1392	1305, 1206	537	C–O: 1145
Calculated	**1**	3305.85	3254.01, 3166.19	1686.02	1621.94	1396.09	1272.79, 1212.90	540.05	–
	2	3305.60	3157.63, 3166.05	1687.11	1627.49	1385.82	1304.89, 1217.73	539.92	C–Cl: 1018.30
	3	3305.84	3193.77, 3164.63	1687.01	1625.90	1386.88	1309.80, 1227.05	540.03	C–F: 1174.13
	4	3306.17	3180.59, 3173.45	1686.69	1625.43	1390.79	1316.32, 1233.65	539.70	O–CH_3: 1021.61
	5	3305.10	3199.50, 3149.26	1686.71	1621.77	1386.85	1307.07, 1211.70	540.42	C–Cl: 1086.38
	6	3305.39	3198.79, 3157.93	1686.72	1623.13	1386.38	1307.25, 1212.66	540.34	C–F: 1135.58
	7	3306.06	3202.40, 3153.90	1685.72	1620.68	1389.12	1312.10, 1214.60	540.55	O–CH_3: 1045.31

ist: isatin, tcrb: thiosemicarbazones, Subs.: Substituent., Scaling factors are ν_{NH} (ist): 0.909, ν_{NH} (tcrb): 0.912, 0.924, $\nu_{C=O}$ (ist): 0.959, $\nu_{C=N}$: 0.911, $\nu_{C=S}$: 0.981, $\nu_{S=C-N}$, ν_{ArC-N}: 0.939, 0.908, ν_{C-I}: 0.965, Subs.: 0.965

Table 4 Experimental and calculated ^{1}H NMR values of the compounds (δ, ppm)

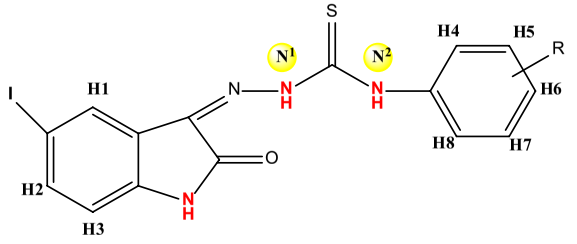

	Comp.	=N–N^{1}H	isatin NH	–N^{2}H–Ar	isatin H1–H3	Ar H4-H8	–CH_2/OCH_3
Experimental	**1**	12.51 (s, 1H)	11.30 (s, 1H)	9.95–9.92 (t, J=6.0 Hz, 1H)	8.00 (s, 1H), 7.66–7.64 (d, J=8.2 Hz, 1H), 6.79–6.77 (d, J=8.2 Hz, 1H)	7.37–7.27 (m, 5H)	4.90–4.88 (d, J=6.0 Hz, 2H)
	2	12.66 (s, 1H)	11.37 (s, 1H)	10.91 (s, 1H)	8.10–8.09 (d, J=1.5 Hz, 1H), 7.70–7.67 (dd, J=8.2, 1.6 Hz, 1H), 6.81–6.79 (d, J=8.2 Hz, 1H)	7.63–7.60 (dd, J=7.6, 1.4 Hz, 1H), 7.53–7.51 (d, J=7.4 Hz, 1H), 7.47–7.39 (m, 2H)	–
	3	12.68 (s, 1H)	11.33 (s, 1H)	10.79 (s, 1H)	8.10–8.09 (d, J=1.6 Hz,1H), 7.70–7.67 (dd, J=8.2, 1.7 Hz, 1H), 6.81–6.79 (d, J=8.2 Hz, 1H)	7.51–7.27 (m, 4H)	–
	4	12.60 (s, 1H)	11.33 (s, 1H)	10.56 (s, 1H)	8.08 (s, 1H), 7.68–7.66 (d, J=8.2 Hz, 1H), 6.80–6.78 (d, J=8.2 Hz, 1H)	7.55–7.53 (d, J=7.7 Hz, 1H), 7.35–7.31 (t, J=7.8 Hz, 1H), 7.16–7.14 (d, J=8.3 Hz, 1H), 7.03–6.99 (t, J=7.6 Hz, 1H)	3.83 (s, 3H)
	5	12.70 (s, 1H)	11.36 (s, 1H)	10.93 (s, 1H)	8.13 (s, 1H), 7.69–7.67 (d, J=8.1 Hz, 1H), 6.80–6.78 (d, J=8.2 Hz, 1H)	7.78 (s, 1H), 7.65–7.63 (d, J=8.1 Hz, 1H), 7.49–7.45 (t, J=7.9 Hz, 1H), 7.36–7.34 (d, J=7.9 Hz, 1H),	–

Table 4 (continued)

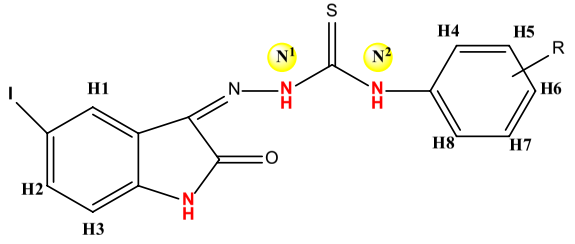

	Comp.	=N–N^{1}H	isatin NH	–N^{2}H–Ar	isatin H1–H3	Ar H4-H8	–CH_2/OCH_3
	6	12.70 (s, 1H)	11.32 (s, 1H)	10.93 (s, 1H)	8.14 (s, 1H), 7.69–7.67 (d, J = 8.2 Hz, 1H), 6.80–6.78 (d, J = 8.2 Hz, 1H)	7.63–7.60 (d, J = 7.8 Hz, 1H), 7.50 (s, 1H), 7.47–7.44 (d, J = 8.1 Hz, 1H), 7.15–7.12 (t, J = 7.5 Hz, 1H)	–
	7	12.65 (s, 1H)	11.35 (s, 1H)	10.86 (s, 1H)	8.16 (s, 1H), 7.70–7.68 (d, J = 8.2 Hz, 1H), 6.81–6.79 (d, J = 8.2 Hz, 1H)	7.37–7.33 (t, J = 8.1 Hz, 1H), 7.27 (s, 1H), 7.23–7.21 (d, J = 8.1 Hz, 1H), 6.88–6.86 (d, J = 8.0 Hz, 1H)	3.79 (s, 3H)
Calculated	**1**	13.22	7.78	8.16	7.85 (H1), 7.82 (H2), 7.21 (H3)	7.96 (H4), 7.96 (H5), 7.93 (H6), 7.94 (H7), 7.97 (H8)	4.39, 5.44 (2H)
	2	13.25	7.85	11.70	8.33 (H1), 7.92 (H2), 7.28 (H3)	8.05 (H5), 7.66 (H6), 7.84 (H7), 10.41 (H8)	–
	3	13.27	7.84	11.18	8.30 (H1), 7.92 (H2), 7.27 (H3)	7.77 (H5), 7.68 (H6), 7.71 (H7), 10.26 (H8)	–
	4	13.04	7.84	11.76	8.38 (H1), 7.91 (H2), 7.28 (H3)	7.50 (H5), 7.68 (H6), 7.45 (H7), 10.04 (H8)	4.16–4.75 (3H)
	5	13.48	7.85	10.75	8.32 (H1), 7.92 (H2), 7.29 (H3)	7.69 (H4), 7.66 (H6), 7.87 (H7), 10.12 (H8)	–
	6	13.32	7.85	10.84	8.32 (H1), 7.93 (H2), 7.28 (H3)	7.41 (H4), 7.40 (H6), 7.91 (H7), 9.97 (H8)	–
	7	13.41	7.84	10.70	8.31 (H1), 7.91 (H2), 7.28 (H3)	7.16 (H4), 7.23 (H6), 7.87 (H7), 9.63 (H8)	3.96–4.24 (3H)

Table 5 Experimental and calculated ^{13}C NMR data of compounds **1–7**, (δ/ppm)

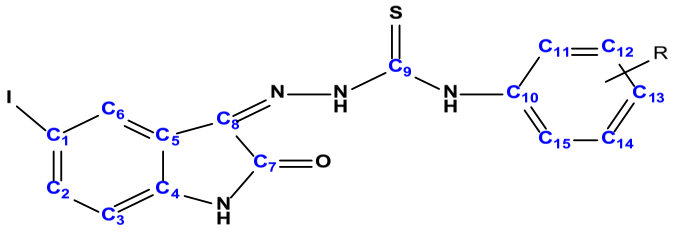

		C1	C2	C3	C4	C5	C6	C7	C8	C9	C10	C11	C12	C13	C14	C15	Subs.
Experimental	**1**	85.7	139.4	123.0	131.0	113.9	129.3	162.5	142.3	178.2	138.8	127.8	128.8	127.5	128.8	127.8	47.7[(a)]
	2	85.9	139.7	122.9	131.2	113.9	129.5	162.5	142.6	178.2	132.1	136.5	128.1	130.1	129.8	131.6	–
	3	85.8	139.7	122.9	130.7	113.9	129.6	162.5	142.6	178.5	126.9 126.7	159.1 156.6	116.6 116.4	131.7 131.6	125.0 124.9	129.8 129.7	–
	4	85.9	139.6	122.9	131.1	113.9	129.7	162.5	142.4	177.4	128.5	154.4	112.4	128.6	120.6	127.4	56.2[(b)]
	5	85.9	139.8	122.8	131.7	113.9	129.9	162.6	142.5	176.8	140.3	125.7	132.9	126.4	130.5	124.7	–
	6	85.9	139.9	122.8	131.6	121.9	129.9	163.3	142.5	176.7	140.5 140.4	114.1 113.9	162.6 160.9	113.0 112.8	130.5 130.4	113.4 113.2	
	7	85.9	139.7	122.9	131.3	113.9	129.9	162.6	142.4	176.6	139.9	111.8	159.7	112.2	129.7	118.2	55.7[(b)]
Calculated	**1**	133.1	147.8	120.0	152.2	131.7	136.3	172.2	137.8	189.5	148.0	139.1	137.9	137.2	137.6	139.1	55.4[(a)]
	2	133.6	148.5	120.3	152.7	131.5	137.1	172.3	137.8	186.2	145.4	138.3	139.1	134.0	136.3	126.0	–
	3	133.6	148.5	120.3	152.6	131.5	136.9	172.3	137.9	185.8	137.0	166.3	123.2	134.0	132.9	126.1	–
	4	133.4	148.1	120.2	152.4	131.8	136.7	172.2	137.0	184.7	136.8	160.4	116.8	134.0	127.2	124.5	59.5[(b)]
	5	133.5	148.5	120.3	152.6	131.4	136.9	172.4	138.0	186.0	150.5	128.7	150.3	133.7	139.3	122.8	–
	6	133.6	148.5	120.2	152.6	131.5	136.9	172.3	137.8	186.0	150.9	114.6	177.2	119.7	139.9	120.3	
	7	133.4	148.2	120.2	152.4	131.5	136.7	172.3	137.6	185.5	150.2	115.4	172.5	114.0	139.2	115.9	59.3[(b)]

Subs.: Substituents, a: CH_2, b: OCH_3

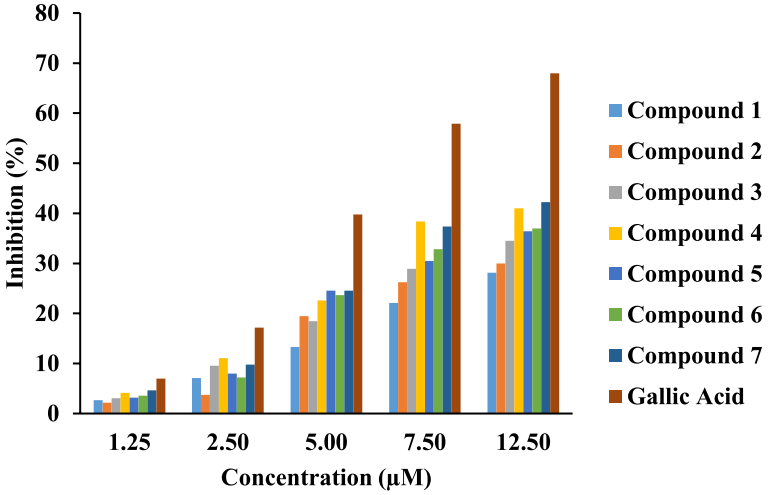

Fig. 1 Percent of inhibition calculated by the DPPH· method for gallic acid and compounds **1–7**

2–Cl (136.5 ppm), 2–F (159.1 ppm), 2–OCH_3 (154.4 ppm), 3–Cl (132.9 ppm), 3–F (162.6 ppm), and 3–OCH_3 (159.7 ppm), present on the aromatic ring. These values agree the data that reported of similar compounds [9, 21, 23, 68].

Antioxidant activity studies

To evaluate the antioxidant properties of the synthesized compounds, concentration-dependent inhibition changes were measured using the DPPH· scavenging method. Gallic acid was used as the standard antioxidant, and the percent inhibition changes obtained for all compounds are shown in Fig. 1. All synthesized compounds showed lower inhibition than gallic acid at all concentrations. When percent inhibitions were examined, compound **7** showed the highest increase, and compound **1** displayed the lowest increase at almost every concentration. Especially at the two highest concentrations (7.50 and 12.50 µM), the compounds showed percent inhibition in the order of **1**, **2**, **3**, **5**, **6**, **4,** and **7** from small to large. This variation is thought to be largely dependent on the location and structure of the thiosemicarbazone-associated substituents.

To compare and evaluate the antioxidant properties of the compounds, IC_{50} values were calculated from the inhibition percentages obtained for five different concentrations, which are presented in Table 6. It was seen that the free radical scavenging effects of the compounds were in the order of **Gallic acid > 7 > 4 > 6 > 5 > 3 > 2 > 1**. In this study, thiosemicarbazone structures with different substituents (−Cl, −F, $-OCH_3$) played an active role in the change of antioxidant activity. Consistent with the findings reported by Andreani et al. [10], the methoxy thiosemicarbazone structures in this study exhibited better antioxidant activity than the halogen-containing structures, as in our study. Compound **1** has the lowest antioxidant activity (See Support B for data and graphs of IC_{50} values).

Table 6 IC_{50} values for gallic acid and the synthesized compounds **1–7**

Comp.	DPPH scavenging activity IC_{50} (μM)*	R^2
1	22.46 ± 0.05	0.957
2	19.30 ± 0.04	0.859
3	18.76 ± 0.04	0.927
4	15.80 ± 0.03	0.877
5	17.71 ± 0.03	0.875
6	16.92 ± 0.03	0.870
7	15.36 ± 0.03	0.896
Gallic Acid	10.13 ± 0.02	0.911

*IC_{50} = the concentration (μM) exhibiting 50% inhibition of DPPH radical

Values are expressed as means ($n = 3$)

In another study, it was reported that methoxy-substituted compounds showed much stronger antioxidant activity than the others [69]. Similarly, in this study, the contribution of substituents to antioxidant activity was observed in the order of $-OCH_3 > -F > -Cl$, regardless of whether they were attached to the *ortho* or *meta* position on the molecule.

Compounds **2**–**4** bound in *ortho* position exhibited lower antioxidant activity than compounds **5**–**7** bound in *meta* position. This observation is consistent with previous findings in the literature. Bakır and Lawag [10] reported similar results for Schiff bases derived from thiocarbohydrazide, isatin, and substituted aldehydes, noting that *meta*-methoxy substitution enhanced antioxidant activity. Moreover, Muğlu et al. also observed that benzaldehyde-derived compounds containing *meta*-substituted groups exhibited higher antioxidant activity [70].

DFT analysis

The LUMO distributions of the compounds are not significantly affected by the substituents and their positions; however, the most notable change in the HOMOs was observed when MeO was at the *ortho* position. Among the two groups of compounds, only *o*-MeO was calculated to localize the HOMOs on the benzene ring (see Fig. 2; for all, refer to Supplementary A, Fig. S22). The localization of the HOMO on the benzene ring suggests that the increased electron density in this region may enhance the molecule's tendency to donate electrons. The *ortho*-methoxy substitution can also contribute to π-conjugation, potentially leading to better orbital overlap and increased nucleophilicity, and this may be associated with the compound's radical scavenging property. This suggests that compound **4** may exhibit a different inhibition effect behavior compared to the other compounds in the groups. At this point, Fig. 1 reveals that, in line with this expectation, the *o*-MeO substituted compound **4** exhibits a higher inhibition effect compared to the chlorine- and fluorine-substituted compounds in both groups, although it should be noted that the *meta*-substituted methoxy compound **7** shows the highest activity of all.

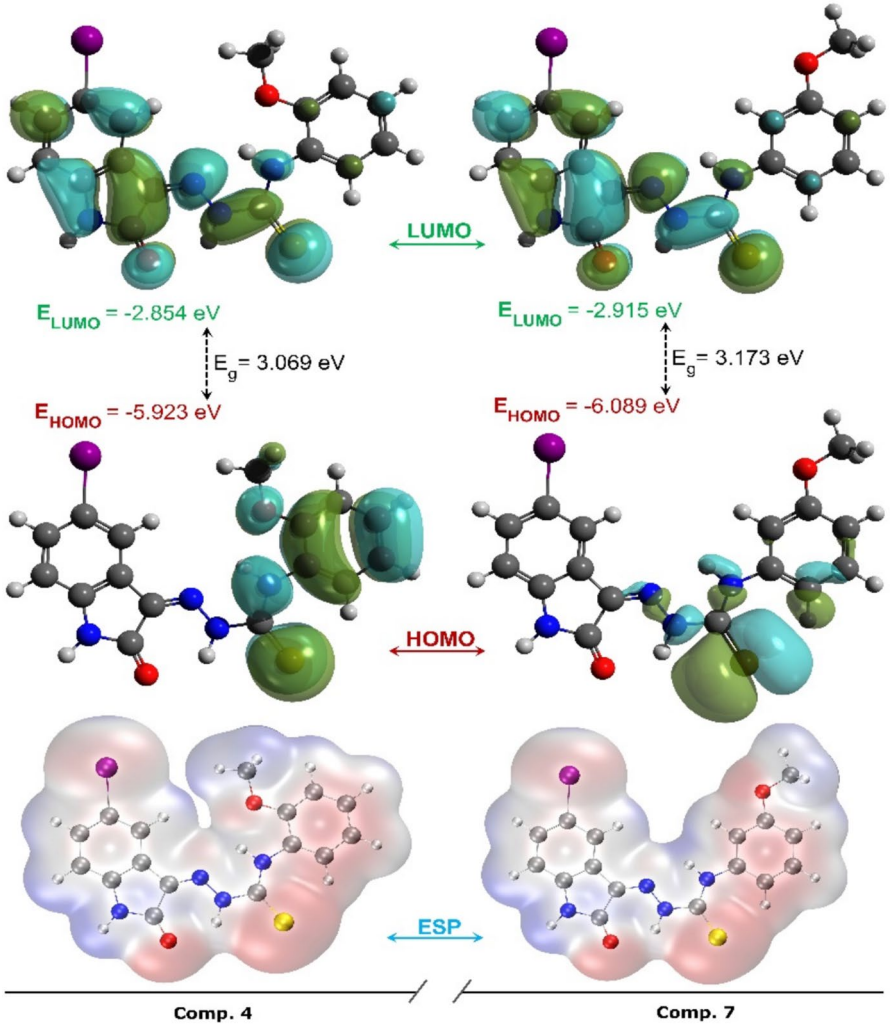

Fig. 2 ESP and HOMO–LUMO maps of compounds **4** and **7**

The calculations indicated that compound **4** exhibits the highest HOMO energy among the tested compounds. While the HOMO energies of all other compounds were below − 6 eV, only compound **4** showed a higher value of − 5.923 eV (Table 7). The energy of the HOMO is an indication of how likely the molecule is to donate an electron. The relationship between the high HOMO energy of compound **4** and its inhibition effect can be considered through SET reactions; however, compound **7** (IC_{50} = 15.36 µM), despite having a lower HOMO energy (− 6.089 eV), exhibits slightly higher activity. This finding supports the idea that, in addition to HOMO energy, other parameters, such as minor differences in steric hindrance, solvation effects, hydrogen atom transfer (HAT), proton-coupled electron transfer (PCET), or

Table 7 Calculated electronic parameters of the compounds

Comp.	E_{HOMO}(eV)	E_{LUMO}(eV)	E_g(eV)	η(eV)	χ(eV)	Ω (eV)	μ *Debye*	ω^- (eV)
1	− 6.009	− 2.832	3.177	1.589	4.421	6.150	4.86237	5.683
2	− 6.240	− 2.969	3.271	1.635	4.605	6.483	3.51961	5.953
3	− 6.233	− 2.967	3.266	1.633	4.600	6.480	3.64706	5.948
4	− 5.923	− 2.854	3.069	1.535	4.389	6.275	5.63618	5.715
5	− 6.277	− 3.056	3.221	1.611	4.667	6.761	4.45655	6.116
6	− 6.266	− 3.047	3.219	1.610	4.656	6.735	4.44237	6.098
7	− 6.089	− 2.915	3.173	1.587	4.502	6.386	4.21724	5.841

E_g: $E_{LUMO} - E_{HOMO}$, η: Chemical Hardness, χ: Electronegativity, ω: Electrophilic index, μ: Dipole moment, ω^-: Electrodonating power

bond dissociation enthalpy (BDE), may also influence the overall antioxidant capacity. On the other hand, compounds containing electron-withdrawing groups (EWGs) such as chlorine and fluorine (compounds **2**, **3**, **5**, and **6**) exhibited lower antioxidant activity. These groups lowered the HOMO energy by withdrawing electrons from the ring through the inductive effect, thereby weakening the molecule's electron-donating capacity.

A higher HOMO energy indicates a greater tendency for the molecule to donate electrons, making it a stronger electron donor and thus more reactive toward electrophiles or radical species. In this context, while the HOMO energies of compounds with substituents in the *meta* position are generally lower than those with substituents in the *ortho* position, and it can be said that compound **5** is more reactive toward electrophiles or radical species than compound **2**, compound **6** more than compound **3**, and compound **7** more than compound **4**. This suggests that for these pairs, lower HOMO energy corresponds to higher antioxidant activity with an inverse relationship. Compared to the *meta* position, the observed increased antioxidant activity for compounds with substituents at the *meta* position (compounds **5**, **6**, and **7**) can be attributed to the easier breaking of the N–H-bond at this position due to the decreased bond dissociation enthalpy (BDE). The order of activity for the compound pairs was **7** > **4**, **6** > **3**, and **5** > **2**, which corresponds to the inverse relationship with their IC_{50} values (IC_{50}: **7** < **4**, **6** < **3**, and **5** < **2**). This inverse relationship with the HOMO energy suggests that the single electron transfer (SET) mechanism may not be the sole dominant pathway in the antioxidant effect of these compounds.

As is known, the HOMO–LUMO energy difference plays an important role in determining the chemical reactivity of a molecule, and the observed antioxidant activities are compatible with lower E_g values in halogen-substituted compounds (compounds **5** and **2**, compounds **6** and **3**), but this correlation was not observed for methoxy-substituted compounds **7** and **4**. This difference may be due to the electron-donating nature of the methoxy group producing electronic effects that differ from the electron-withdrawing properties of the halogen atoms. While halogen atoms tend to widen the HOMO–LUMO energy gap by withdrawing electron density from the π-electron system through their inductive effects, the methoxy group, through its mesomeric effect, donates electron density to the π-electron system, thus influencing

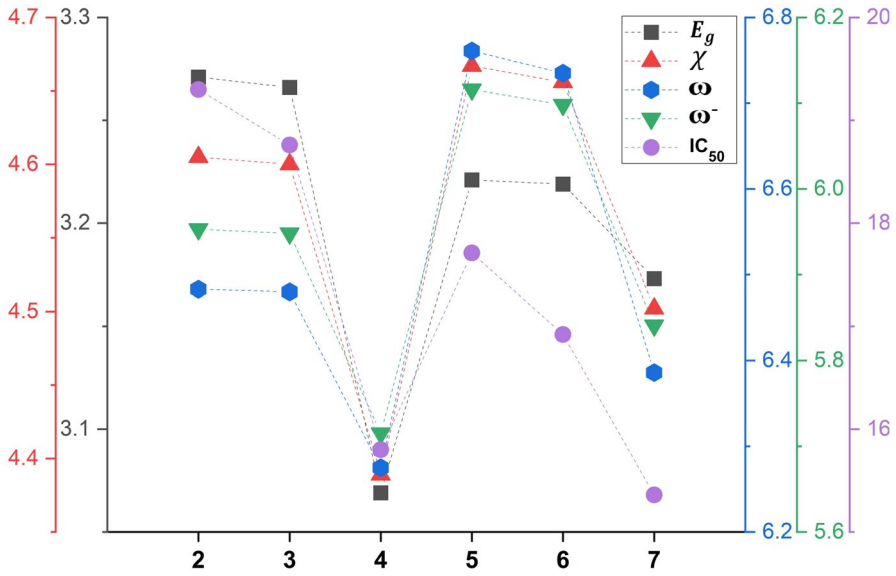

Fig. 3 Calculated electronic parameters vs IC_{50} values of the compounds **2–7**

this energy gap in the opposite direction. Therefore, the opposing electronic effects between the methoxy and halogen substituents may be one of the reasons for the observed E_g differences. In addition, in general, an inverse correlation is observed between the electronegativity (χ), electrophilicity index (ω), and electrodonating power (ω^-) values of the compounds and their antioxidant activity (Fig. 3). Compounds with higher antioxidant activity (lower IC_{50}) usually possess lower electronic index values. This observation supports the insight that antioxidant activity is related to the electron-donating and nucleophilic properties of the compounds, and that an increase in their electrophilic character reduces this activity.

Urease inhibition assay

The urease inhibitory activity of the compounds was evaluated employing the indophenol assay method. Although no inhibition effect was observed for the *meta*-substituted compounds **5–7**, the *ortho*-substituted compounds **2–4** exhibited higher inhibition than the standard thiourea. This can be attributed to the electronic properties of the substituents in the *ortho* position: chlorine (in compound **2**) and fluorine (in compound **3**) act as strong electron-withdrawing groups, methoxy (in compound **4**) exhibits both electron-withdrawing (as inductive) and donating (as mesomeric) effects. Benzyl group ($C_6H_5CH_2$) in compound **1** primarily functions as an electron-donating group. At this point, it is observed that compounds with strong electron-withdrawing substituents in the *ortho* position exhibit higher inhibitory effects. The order of inhibition activity from highest to lowest is as follows: **2 > 3 > 4 > 1 > thiourea** (Table 8, see Support B for data and graphs of IC_{50} values).

Table 8 Enzyme inhibition activities, binding affinities, and constants of the compounds

Comp.	Inhibition, IC_{50} (μg/mL)	Binding affinity, kcal/mol	Binding constant, μM
1	7.23 ± 0.15^{b}	−5.90	55.20
2	1.62 ± 0.05^{a}	−7.70	2.77
3	1.67 ± 0.10^{a}	−7.50	3.86
4	1.73 ± 0.31^{a}	−7.20	6.36
5	–	−6.60	17.25
6	–	−7.80	2.35
7	–	−6.20	33.53
Thiourea	18.99 ± 0.43^{c}	−3.20	4903.76

Molecular docking protocol

The interactions of the compounds with urease, conventional hydrogen bonding, and pi-alkyl interaction were exhibited in all of them. While carbon-hydrogen bonds were found between compounds **1**, **2**, and **4** and urease, alkyl interactions were observed between compounds **1**, **4**, **5**, **6**, and **7** and urease. In addition, urease and compounds **2** and **3** have pi-pi stacked interactions, urease and compounds **1**, **3**, **4**, **6**, and **7** have pi-cation interactions, and urease and compounds **3**, **4**, **5**, **6**, and **7** have pi-anion interactions. Interactions, halogen interactions between urease and compounds **4**, **5**, and **7**, pi-sulfur and pi–pi T-shaped interactions between urease and compounds **5** and **7**, and pi-sigma interactions between urease and compound **5** were observed (Figs. 4, 5, Tables 9, and 10).

It was observed that thiourea, used as standard, performed conventional hydrogen bonding and pi-sulfur interaction with urease (Fig. 5 and Table 10). Additionally, it was noted that thiourea interacts with amino acids ASP494, ARG609, GLU493, HIS593, HIS492, and HIS519. It has been observed that almost all of the amino acids that thiourea interacts with also interact with other compounds. As seen in Table 8, the binding affinities and constants of the compounds' interactions with urease are compared with thiourea. Compounds **2**, **3**, **4**, and **6** achieved the best binding.

Molecular dynamic (MD) simulations

For the development of drugs, it is necessary to study the dynamic behavior of molecules and complex systems with which they interact. One calculation method used for this purpose is molecular docking simulation (MD simulation). In contrast to conventional molecular docking methods, MD simulations consider the target's flexibility and thus allow a more accurate estimation of the binding energy to identify potential inhibitors [71].

Compounds **5**, **6**, and **7** were not selected for molecular dynamics because their effects on enzyme inhibition were not observed. However, in terms of binding affinities, compound **6** was observed to have a high binding affinity. However, as

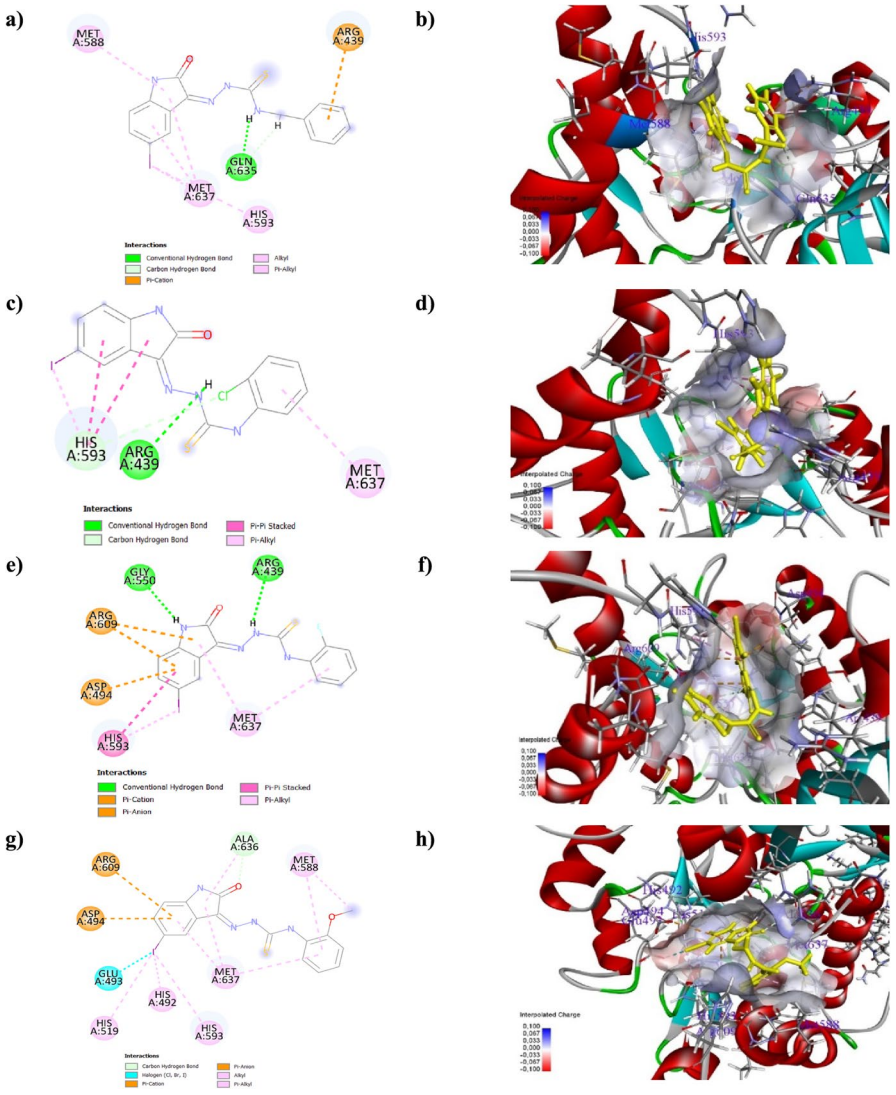

Fig. 4 Molecular docking 2D and 3D-charge images of **1** (**a**), **2** (**c**), **3** (**e**), and **4** (**g**) with urease

we have done in our previous studies, dynamical calculations were performed for the compound that exhibited high activity in both in vitro enzyme inhibition and molecular interaction [72–75]. This study followed the same approach. Therefore, compound **2** was selected because its effect was due to the electron-withdrawing nature of the chlorine atom located at the *ortho* position of compound **2**, which results in only a strong binding interaction with the enzyme's active site, rather than a strong binding interaction.

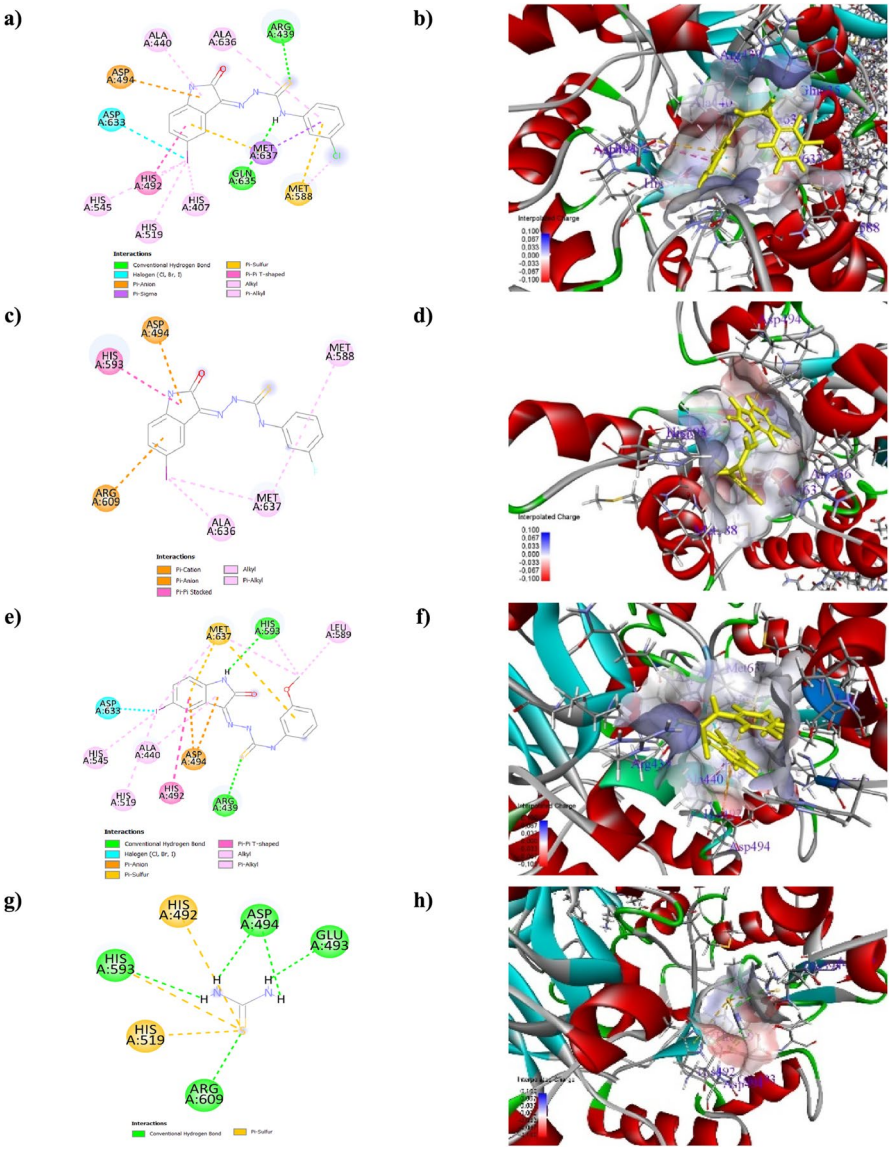

Fig. 5 Molecular docking 2D and 3D-charge images of **5** (**a**), **6** (**c**), **7** (**e**), and thiourea (**g**) with urease

Molecular modeling was used to predict the kinetics and stability of the drug on urease under physiological conditions. High RMSD values suggested that the protein experienced significant structural alterations throughout the simulation, whereas lower RMSD values pointed out that the protein maintained a relatively stable conformation. While compound **2** alone had a constant RMSD of 0.1 nm for 100 ns, the protein started at 0.4 nm and reached 0.6 nm, remaining stable

Table 9 Urease-compounds **1**–**4** interaction categories, species and molecular docking distance

Comp.	Amino acids	Distance	Bond types
1	GLN635	1.93492	Hydrogen Bond (Conventional)
	GLN635	3.07681	Hydrogen Bond (Carbon)
	ARG439	4.3892	Electrostatic (Pi-Cation)
	MET637	4.38651	Hydrophobic (Alkyl)
	HIS593	4.61592	Hydrophobic (Pi-Alkyl)
	MET637	4.82707	Hydrophobic (Pi-Alkyl)
	MET588	4.7279	Hydrophobic (Pi-Alkyl)
	MET637	5.37713	Hydrophobic (Pi-Alkyl)
	ARG439	5.43572	Hydrophobic (Pi-Alkyl)
2	ARG439	2.18602	Hydrogen Bond (Conventional)
	HIS593	3.02629	Hydrogen Bond (Carbon)
	HIS593	4.07396	Hydrophobic (Pi-Pi Stacked)
	HIS593	5.24167	Hydrophobic (Pi-Pi Stacked)
	HIS593	4.17256	Hydrophobic (Pi-Alkyl)
	MET637	4.55556	Hydrophobic (Pi-Alkyl)
3	GLY550	2.92297	Hydrogen Bond (Conventional)
	ARG439	2.11359	Hydrogen Bond (Conventional)
	ARG609	4.47061	Electrostatic (Pi-Cation)
	ARG609	4.73301	Electrostatic (Pi-Cation)
	ASP494	3.49156	Electrostatic (Pi-Anion)
	HIS593	4.54648	Hydrophobic (Pi-Pi Stacked)
	HIS593	3.66536	Hydrophobic (Pi-Alkyl)
	MET637	5.3258	Hydrophobic (Pi-Alkyl)
	MET637	5.4818	Hydrophobic (Pi-Alkyl)
4	ALA636	2.60654	Hydrogen Bond (Carbon)
	GLU493	3.29522	Halogen (Cl, Br, I)
	ARG609	4.76982	Electrostatic (Pi-Cation)
	ASP494	4.75214	Electrostatic (Pi-Anion)
	MET588	4.01219	Hydrophobic (Alkyl)
	HIS492	4.84862	Hydrophobic (Pi-Alkyl)
	HIS519	4.0705	Hydrophobic (Pi-Alkyl)
	HIS593	4.77311	Hydrophobic (Pi-Alkyl)
	MET637	5.15634	Hydrophobic (Pi-Alkyl)
	ALA636	4.42734	Hydrophobic (Pi-Alkyl)
	MET637	4.97263	Hydrophobic (Pi-Alkyl)
	MET588	5.19763	Hydrophobic (Pi-Alkyl)
	MET637	4.57639	Hydrophobic (Pi-Alkyl)

for 100 ns. Fluctuations were observed in the complex. It remained constant at 0.4 nm for 50 ns, then reached 1.0 nm after 50 ns and until 95 ns, but decreased to 0.6 nm for 100 ns (Fig. 6a). The low RMSD of the complex indicates that the

Table 10 Urease-compounds **5**–**7**, thiourea interaction categories, species and molecular docking distance

Comp.	Amino acids	Distance	Bond types
5	ARG439	2.83362	Hydrogen Bond (Conventional)
	ARG439	2.49462	Hydrogen Bond (Conventional)
	GLN635	2.32922	Hydrogen Bond (Conventional)
	ASP633	3.29981	Halogen (Cl, Br, I)
	ASP494	4.86043	Electrostatic (Pi-Anion)
	MET637	2.92704	Hydrophobic (Pi-Sigma)
	MET588	4.62849	Other (Pi-Sulfur)
	MET637	4.39611	Other (Pi-Sulfur)
	HIS492	5.63432	Hydrophobic (Pi-Pi T-shaped)
	MET588	4.29342	Hydrophobic (Alkyl)
	HIS407	5.3766	Hydrophobic (Pi-Alkyl)
	HIS492	5.29397	Hydrophobic (Pi-Alkyl)
	HIS519	4.58542	Hydrophobic (Pi-Alkyl)
	HIS545	4.3787	Hydrophobic (Pi-Alkyl)
	ALA440	4.77375	Hydrophobic (Pi-Alkyl)
	ALA636	5.24876	Hydrophobic (Pi-Alkyl)
6	ARG609	4.81218	Electrostatic (Pi-Cation)
	ASP494	3.94056	Electrostatic (Pi-Anion)
	HIS593	4.02075	Hydrophobic (Pi-Pi Stacked)
	ALA636	4.3933	Hydrophobic (Alkyl)
	MET637	4.4016	Hydrophobic (Alkyl)
	MET588	5.21953	Hydrophobic (Pi-Alkyl)
	MET637	4.61509	Hydrophobic (Pi-Alkyl)
7	ARG439	2.71887	Hydrogen Bond (Conventional)
	HIS593	2.72467	Hydrogen Bond (Conventional)
	ASP633	3.09248	Halogen (Cl, Br, I)
	ASP494	4.98672	Electrostatic (Pi-Anion)
	ASP494	4.69828	Electrostatic (Pi-Anion)
	MET637	4.39039	Other (Pi-Sulfur)
	MET637	5.68288	Other (Pi-Sulfur)
	HIS492	5.66208	Hydrophobic (Pi-Pi T-shaped)
	MET637	4.50712	Hydrophobic (Alkyl)
	LEU589	4.37699	Hydrophobic (Alkyl)
	MET637	4.1132	Hydrophobic (Alkyl)
	HIS519	4.74882	Hydrophobic (Pi-Alkyl)
	HIS545	4.2995	Hydrophobic (Pi-Alkyl)
	HIS593	4.14918	Hydrophobic (Pi-Alkyl)
	ALA440	4.66972	Hydrophobic (Pi-Alkyl)

Table 10 (continued)

Comp.	Amino acids	Distance	Bond types
Thiourea	ARG609	2.70851	Hydrogen Bond (Conventional)
	ASP494	2.21705	Hydrogen Bond (Conventional)
	GLU493	2.21907	Hydrogen Bond (Conventional)
	HIS593	3.03287	Hydrogen Bond (Conventional)
	ASP494	2.54566	Hydrogen Bond (Conventional)
	HIS492	5.16122	Other (Pi-Sulfur)
	HIS519	4.3884	Other (Pi-Sulfur)
	HIS593	4.96991	Other (Pi-Sulfur)

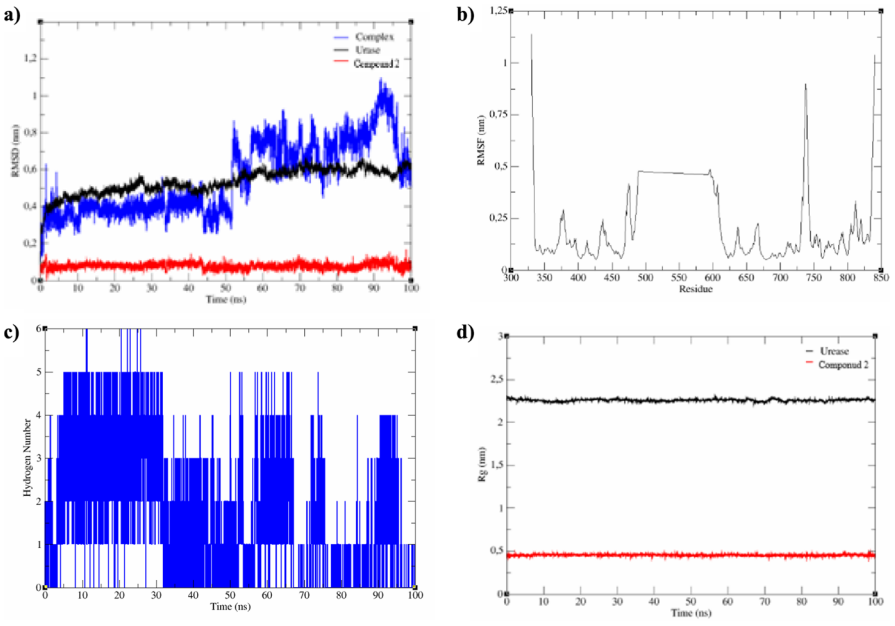

Fig. 6 RMSD (**a**) and RMSF (**b**) H-bond interactions (**c**), and Rg plotting (**d**) with compound **2**-urease

protein maintains its stable conformation. In other words, the complex remains stable for 100 ns. This supports molecular interaction studies.

The root-mean-square fluctuation (RMSF) method calculates the variations of each amino acid residue with and without specific ligand molecules during the simulation process. Starting from the Cα atoms of urease, the RMSF for all complex systems showed that the intensity of the fluctuation was within 0.1–1.0 nm (Fig. 6b). Consequently, the RMSF plots showed the protein structure's stability and the presence of flexible regions required to reach the optimal states.

To determine the stability of a ligand-receptor complex, it was essential to investigate the binding interactions between proteins and ligands during MD simulations [76]. The H-bond formed by the ligands and urease during the 100-ns MD simulations is shown in Fig. 6c. During the MD simulations, the H-bonds of the complex changed between two and six constantly.

The degree of compactness of a protein is represented by its Rg. The Rg is a convenient and reliable indicator of a drug's ability to alter protein structure. The loose molecular packing of a protein is represented by its Rg value. The dynamics calculations for 100 ns of urease and the compound were consistently around 2.25 and 0.45 nm, respectively, as shown in Fig. 6d.

Conclusion

In this work, novel 5-iodoisatin-thiosemicarbazone derivatives were synthesized with excellent yields ranging from 60 to 95%. The structural characterization of the compounds was carried out using various spectroscopic techniques, including FT-IR, ^{1}H NMR, and ^{13}C NMR spectroscopy, as well as elemental analysis.

The synthesized compounds' antioxidant activity was assessed through the free radical scavenging (DPPH·) assay as in vitro. The IC_{50} values for these compounds varied between 15.36 and 22.46 µM. These values are close to the IC_{50} value of gallic acid (10.13 µM), which is used as a standard. The results indicate that the antioxidant activities of the synthesized compounds are comparable to that of gallic acid, indicating that they do not exhibit very weak activity. Furthermore, it was observed that the antioxidant activities of the compounds varied depending on different substituent groups, with *meta*-substituted groups exhibiting higher antioxidant activity than *ortho*-substituted groups.

DFT calculations have revealed some information about the structural and electronic properties of the substituents and their relationship with antioxidant activity. The observed changes in HOMO energies, particularly the effect of *ortho*-methoxy substitution, highlight the importance of substituent position and type in determining the electron-donating ability and reactivity of these compounds. The findings also showed a strong relationship between different electronic parameters (such as E_g, electronegativity, electrophilic index, and electrodonating power) and their effects on antioxidant activity.

Following an analysis of the samples' urease inhibition and interactions with urease, it was found that compound **2** exhibited the best inhibition effect (IC_{50}, 1.62 ± 0.05 µg/mL, and -7.70 kcal/mol). While the *meta*-substituted compounds **5–7** showed no inhibitory effect, the *ortho*-substituted compounds **2–4** showed more inhibition than the standard thiourea. Besides, the state of the complex formed by compound number **2**, which has the best urease inhibition activity and is supported by molecular dynamics simulation. Furthermore, molecular docking simulations were employed to investigate the interaction of the newly synthesized compounds with the active site of the target enzyme. Alkyl connections were noted between compounds **1**, **4**, **5**, **6**, and **7** and urease, whereas carbon-hydrogen linkages were discovered between compounds **1**, **2**, and **4**. Consequently, the synthesized compounds

hold promise as potential candidates for future in vivo works as pharmacological and biological agents. Additionally, molecules incorporating the isatin-thiosemicarbazone scaffold may have wide applications in both biochemistry and medicine fields.

Supplementary Information The online version contains supplementary material available at https://doi.org/10.1007/s11164-025-05761-8.

Acknowledgements I want to thank the Scientific and Technological Research Applications and Center (Tokat Gaziosmanpaşa University, Gübitam) and Dr. Ömer Faruk Ensari for taking the NMR spectra. IR, ^{1}H NMR, and ^{13}C NMR spectra of all compounds are given in the supporting information. The DFT calculations reported in this paper were partially performed at TUBITAK ULAKBIM, High Performance and Grid Computing Center (TRUBA resources).

Author contributions H.Y.: Spectroscopic Characterization, Writing–Review, Visualization and Editing. H.M.: Synthesis, Characterization, Writing–Review. T.K.B.: Biological studies, Writing–Review. S.Y.: Biological studies, Molecular Docking and Dynamics, Writing–Review. A.G.A.M.: Biological studies, Writing–Review. M.S.Ç.: DFT Calculations, Writing–Review. T. Ö.: Biological studies, Molecular Docking and Dynamics, Writing–Review. All authors reviewed the manuscript.

Funding This research did not receive any specific grant from funding agencies in the public, commercial, or not-for-profit sectors.

Data availability No datasets were generated or analysed during the current study.

Declarations

Competing interests The authors declare no competing interests.

Ethics approval All of the material is owned by the authors, and/or no permissions are required.

References

1. A. Jarrahpour, D. Khalili, E. De Clercq, C. Salmi, J. Brunel, Synthesis, antibacterial, antifungal and antiviral activity evaluation of some new bis-Schiff bases of isatin and their derivatives. Molecules **12**, 1720 (2007)
2. S. Pandeya, D. Sriram, G. Nath, E. DeClercq, Synthesis, antibacterial, antifungal and antiviral activity evaluation of some new bis-Schiff bases of isatin and their derivatives. Eur. J. Pharm. Sci. **9**, 25 (1999)
3. M. Premanathan, S. Radhakrishnan, K. Kulangiappar, G. Singaravelu, V. Thirumalaiarasu, T. Sivakumar, K. Kathiresan, Antioxidant & anticancer activities of isatin (1H-indole-2, 3-dione), isolated from the flowers of *Couroupita guianensis* Aubl. Indian J. Med. Res. **136**, 822 (2012)
4. M.S.S. Adam, Z.H. Al-Ateya, M.M. Makhlouf, O.S. Abdel-Rahman, A. Shtaiwi, A. Khalil, Substituent effect on the chemical and biological properties of diisatin dihydrazone Schiff bases: DFT and docking studies. Comput. Biol. Chem. **113**, 108190 (2024)
5. D. Sriram, P. Yogeeswari, K. Meena, Semiexperimental equilibrium structure of 1-methylisatin from gas-phase electron diffraction data and structural changes in isatin due to 1-methyl and 5-fluoro substituents as predicted by coupled cluster computations. Die Pharm. Int. J. Pharm. Sci. **61**, 274 (2006)
6. T. Aboul-Fadl, F.A. Bin-Jubair, O. Aboul-Wafa, Schiff bases of indoline-2, 3-dione (isatin) derivatives and nalidixic acid carbohydrazide, synthesis, antitubercular activity and pharmacophoric model building. Eur. J. Med. Chem. **45**, 4578 (2010)
7. B. Sridhar, G. Nagesh, K. Prashantha, M. Yamuna, S. Sanjay, K. Srinath, K. Ranjinikanth, R. Gani, R. Nalini, S. Basavarajaiah, Discovery of novel isatin encompassing oxadiazoles as potential

inhibitors against New Delhi metallo-β-lactamase-1: synthesis, spectral analysis, antimicrobial, and molecular modeling studies. Russ. J. Bioorg. Chem. **50**, 1376 (2024)
8. H. Yakan, M.S. Çavuş, B.Z. Kurt, H. Muğlu, F. Sönmez, E. Güzel, A new series of asymmetric bis-isatin derivatives containing urea/thiourea moiety: Preparation, spectroscopic elucidation, antioxidant properties and theoretical calculations. J. Mol. Struct. **1239**, 130495 (2021)
9. G. Kiran, M. Sarangapani, T. Gouthami, A.R.N. Reddy, Synthesis, characterization, and antimicrobial and antioxidant activities of novel bis-isatin carbohydrazone derivatives. Toxicol. Environ. Chem. **95**, 367 (2013)
10. A. Andreani, S. Burnelli, M. Granaiola, A. Leoni, A. Locatelli, R. Morigi, M. Rambaldi, L. Varoli, M.A. Cremonini, G. Placucci, New isatin derivatives with antioxidant activity. Eur. J. Med. Chem. **45**, 1374 (2010)
11. T.K. Bakır, J.B. Lawag, Preparation, characterization, antioxidant properties of novel Schiff bases including 5-chloroisatin-thiocarbohydrazone. Res. Chem. Intermed. **46**, 2541 (2020)
12. T.R. Bal, B. Anand, P. Yogeeswari, D. Sriram, Synthesis and evaluation of anti-HIV activity of isatin β-thiosemicarbazone derivatives. Bioorg. Med. Chem. Lett. **15**, 4451 (2005)
13. C.R. Prakash, S. Raja, G. Saravanan, Synthesis, characterization and anticonvulsant activity of novel Schiff base of isatin derivatives. Int J Pharm Pharm Sci **2**, 177 (2010)
14. U. Kulandaivelu, V.G. Padmini, K. Suneetha, B. Shireesha, J.V. Vidyasagar, T.R. Rao, J. Kn, A. Basu, V. Jayaprakash, Synthesis, antimicrobial and anticancer activity of new thiosemicarbazone derivatives. Arch. Pharm. (Weinheim) **344**, 84 (2011)
15. B. Rogalewicz, M. Pitucha, M. Świątkowski, E. Humeniuk, G. Adamczuk, M. Drózd, Z. Karczmarzyk, E. Kuśmierek, K. Strzelec, A. Raducka, Structure-activity relationship and cytotoxicity of the new thiosemicarbazide derivatives and their Cu(II) complexes against prostate and melanoma cancer cells. Arch. Biochem. Biophys. **755**, 109955 (2024)
16. D.L. Sun, S. Poddar, R.D. Pan, E.W. Rosser, E.R. Abt, J. Van Valkenburgh, T.M. Le, V. Lok, S.P. Hernandez, J. Song, Isoquinoline thiosemicarbazone displays potent anticancer activity with in vivo efficacy against aggressive leukemias. RSC Med. Chem. **11**, 392 (2020)
17. H. Pervez, N. Manzoor, M. Yaqub, A. Khan, K.M. Khan, F.-u-H. Nasim, M.I. Choudhary, Synthesis and urease inhibitory properties of some new N4-substituted 5-nitroisatin-3-thiosemicarbazones. Lett. Drug Des. Discov. **7**, 102 (2010)
18. Z. Bakherad, H. Bakherad, S. Sepehri, M.A. Faramarzi, K. Mahnam, S. Mojtabavi, M. Mahdavi, In silico and in vitro studies of thiosemicarbazone-indole hybrid compounds as potent α-glycosidase inhibitors. Comput. Biol. Chem. **97**, 107642 (2022)
19. G. Jasinski, E. Salas-Sarduy, D. Vega, L. Fabian, M.F. Martini, A.G. Moglioni, Thiosemicarbazone derivatives: evaluation as cruzipain inhibitors and molecular modeling study of complexes with cruzain. Biorg. Med. Chem. **61**, 116708 (2022)
20. N. Solak, S. Rollas, Synthesis and antituberculosis activity of 2-(aryl/alkylamino)-5-(4-aminophenyl)-1, 3, 4-thiadiazoles and their Schiff bases. ARKIVOC **12**, 173 (2006)
21. H. Yakan, Preparation, structure elucidation, and antioxidant activity of new bis (thiosemicarbazone) derivatives. Turk. J. Chem. **44**, 1085 (2020)
22. A. Božić, N. Filipović, I. Novakovic, S. Bjelogrlić, J. Nikolić, S. Drmanić, A. Marinković, Synthesis, antioxidant and antimicrobial activity of carbohydrazones. J. Serb. Chem. Soc. **82**, 495 (2017)
23. K.H.D. Reddy, S.-M. Lee, K. Seshaiah, R.K. Babu, Synthesis, characterization of thiosemicarabzone metal complexes and antioxidant activity in different in vitro model systems. J. Serb. Chem. Soc. **78**, 229 (2013)
24. V. Manakkadan, J. Haribabu, V.N.V. Palakkeezhillam, P. Rasin, R. Vediyappan, V.S. Kumar, M. Garg, N. Bhuvanesh, A. Sreekanth, Molecular and biomolecular spectroscopy. Spectrochim. Acta Part A Mol. Biomol. Spectrosc. **313**, 124117 (2024)
25. X. Jia, Q. Liu, S. Wang, B. Zeng, G. Du, C. Zhang, Y. Li, Synthesis, cytotoxicity, and in vivo antitumor activity study of parthenolide semicarbazones and thiosemicarbazones. Biorg. Med. Chem. **28**, 115557 (2020)
26. A.Y. Lukmantara, D.S. Kalinowski, N. Kumar, D.R. Richardson, Structure–activity studies of 4-phenyl-substituted 2′-benzoylpyridine thiosemicarbazones with potent and selective anti-tumour activity. Org. Biomol. Chem. **11**, 6414 (2013)
27. A. Karaküçük-İyidoğan, D. Taşdemir, E.E. Oruç-Emre, J. Balzarini, Novel platinum(II) and palladium(II) complexes of thiosemicarbazones derived from 5-substitutedthiophene-2-carboxaldehydes and their antiviral and cytotoxic activities. Eur. J. Med. Chem. **46**, 5616 (2011)

28. B.N. Brousse, R. Massa, A.G. Moglioni, M. Martins Alho, G. Gutkind, G.Y. Moltrasio, Antibacterial and antifungal activity of some thiosemicarbazones and 1, 3, 4-thiadiazolines. J. Chil. Chem. Soc. **49**, 45 (2004)
29. M. Tahriri, M. Yousefi, K. Mehrani, M. Tabatabaee, M.D. Ashkezari, Synthesis, characterization and antimicrobial activity of two novel sulfonamide Schiff base compounds. Pharm. Chem. J. **51**, 425 (2017)
30. S. Shankerrao, Y.D. Bodke, S.S. Mety, Synthesis, antioxidant, and antibacterial studies of phenolic esters and amides of 2-(1-benzofuran-2-yl) quinoline-4-carboxylic acid. Med. Chem. Res. **22**, 1163 (2013)
31. K. Krumova, G. Cosa, Overview of reactive oxygen species. Singlet Oxyg. Appl. Biosci. Nanosci. **1**, 1 (2016)
32. F. Begum, N.B. Almandil, M.A. Lodhi, K.M. Khan, A. Hameed, S. Perveen, Synthesis and urease inhibitory potential of benzophenone sulfonamide hybrid in vitro and in silico. Bioorg. Med. Chem. **27**, 1009 (2019)
33. H. Yakan, H.-H. Omer, O. Buruk, Ş Çakmak, S. Marah, A. Veyisoğlu, H. Muğlu, T. Ozen, H. Kütük, Synthesis, structure elucidation, biological activity, enzyme inhibition and molecular docking studies of new Schiff bases based on 5-nitroisatin-thiocarbohydrazone. J. Mol. Struct. **1277**, 134799 (2023)
34. H. Yakan, S. Ozturk, E.U. Tolgay, S. Yenigun, S. Marah, T. Doruk, T. Ozen, H. Kutuk, Kinetic studies, antioxidant activities, enzyme inhibition properties and molecular docking of 1, 3-dihydro-1, 3-dioxoisoindole derivatives. Acta Chim. Slov. **70**, 29 (2023)
35. Ş Çakmak, Novel diamide derivatives: synthesis, characterization, urease inhibition, antioxidant, antibacterial, and molecular docking studies. J. Mol. Struct. **1261**, 132932 (2022)
36. P. Kosikowska, Ł Berlicki, Urease inhibitors as potential drugs for gastric and urinary tract infections: a patent review. Expert Opin. Ther. Pat. **21**, 945 (2011)
37. X.-Y. Jiang, L.-Q. Sheng, C.-F. Song, N.-N. Du, H.-J. Xu, Z.-D. Liu, S.-S. Chen, Mechanism, kinetics, and antimicrobial activities of 2-hydroxy-1-naphthaldehyde semicarbazone as a new Jack bean urease inhibitor. New J. Chem. **40**, 3520 (2016)
38 H. Steinhagen, The evolution of drug discovery: from traditional medicines to modern drugs, in *ChemMedChem*. ed. by E. Raviña (Wiley, Weinheim, 2011), p.1746
39. R.A. Finch, M.-C. Liu, S.P. Grill, W.C. Rose, R. Loomis, K.M. Vasquez, Y.-C. Cheng, A.C. Sartorelli, Triapine (3-aminopyridine-2-carboxaldehyde-thiosemicarbazone): a potent inhibitor of ribonucleotide reductase activity with broad spectrum antitumor activity. Biochem. Pharmacol. **59**, 983 (2000)
40. R.W. Brockman, J.R. Thomson, M.J. Bell, H.E. Skipper, Observations on the antileukemic activity of pyridine-2-carboxaldehyde thiosemicarbazone and thiocarbohydrazone. Cancer Res. **16**, 167 (1956)
41. M. Ahmad, H. Pervez, S. Zaib, M. Yaqub, M.M. Naseer, S.U. Khan, J. Iqbal, Synthesis, biological evaluation and docking studies of some novel isatin-3-hydrazonothiazolines. RSC Adv. **6**, 60826 (2016)
42. V. Bondet, W. Brand-Williams, C. Berset, Kinetics and mechanisms of antioxidant activity using the DPPH. free radical method. LWT Food Sci. Technol. **30**, 609 (1997)
43. N. Yaylı, G. Kılıç, N. Kahriman, Ş Kanbolat, A. Bozdeveci, ŞA. Karaoğlu, R. Aliyazıcıoğlu, H.E. Sellitepe, İS. Doğan, A. Aydın, Synthesis, biological evaluation (antioxidant, antimicrobial, enzyme inhibition, and cytotoxic) and molecular docking study of hydroxy methoxy benzoin/benzil analogous. Bioorg. Chem. **115**, 105183 (2021)
44. H. Yakan, S. Ozturk, E. Uyar Tolgay, S. Yenigun, S. Marah, T. Doruk, T. Ozen, H. Kutuk, Kinetic studies, antioxidant activities, enzyme inhibition properties and molecular docking of 1, 3-dihydro-1, 3-dioxoisoindole derivatives. Acta Chim. Slov. **70**, 29 (2023)
45. H. Yakan, S. Cakmak, H. Kutuk, S. Yenigun, T. Ozen, Synthesis, characterization, antioxidant, and antibacterial activities of new 2, 3-dimethoxy and 3-acetoxy-2-methyl benzamides. Res. Chem. Intermed. **46**, 2767 (2020)
46. W. Brand-Williams, M.-E. Cuvelier, C. Berset, Use of a free radical method to evaluate antioxidant activity. LWT Food Sci. Technol. **28**, 25 (1995)
47. E.N. Frankel, A.S. Meyer, The problems of using one-dimensional methods to evaluate multifunctional food and biological antioxidants. J. Sci. Food Agric. **80**, 1925 (2000)

48. S. Mukherjee, N. Pawar, O. Kulkarni, B. Nagarkar, S. Thopte, A. Bhujbal, P. Pawar, B.M.C. Complement, Evaluation of free-radical quenching properties of standard *Ayurvedic* formulation *Vayasthapana Rasayana*. Altern. Med. **11**, 1 (2011)
49. F. Neese, Software update: the ORCA program system–Version 5.0. WIREs Comput. Mol. Sci. **12**, e1606 (2022)
50. P. Hohenberg, W. Kohn, Inhomogeneous electron gas. Phys. Rev. **136**, B864 (1964)
51. W. Kohn, L.J. Sham, Self-consistent equations including exchange and correlation effects. Phys. Rev. **140**, A1133 (1965)
52. L. Zhang, S.B. Mulrooney, A.F. Leung, Y. Zeng, B.B. Ko, R.P. Hausinger, H. Sun, Inhibition of urease by bismuth(III): implications for the mechanism of action of bismuth drugs. Biometals **19**, 503 (2006)
53. H.M. Berman, J. Westbrook, Z. Feng, G. Gilliland, T.N. Bhat, H. Weissig, I.N. Shindyalov, P.E. Bourne, The protein data bank. Nucleic Acids Res. **28**, 235 (2000)
54. Y. Başar, İ. Demirtaş, S. Yenigün, Y. İpek, T. Özen, L. Behçet, Molecular docking, molecular dynamics, MM/PBSA approaches and bioactivity studies of nepetanudoside B isolated from endemic *Nepeta aristata*. J. Biomol. Struct. Dyn. **43**(11), 5486 (2025)
55. Y. Basar, S. Yenigun, F. Gul, T. Ozen, I.A. Demirtas, M. Hakkı, S. Temel, Phytochemical profiling, molecular docking and ADMET prediction of crude extract of *Atriplex nitens* Schkuhr for the screening of antioxidant and urease inhibitory. Int. J. Chem. Technol. **8**, 62 (2024)
56. S. Yenigün, Y. Başar, Y. İpek, L. Behçet, T. Özen, İ Demirtaş, Determination of antioxidant, DNA protection, enzyme inhibition potential and molecular docking studies of a biomarker ursolic acid in Nepeta species. J. Biomol. Struct. Dyn. **42**, 5799 (2024)
57. S. Yenigun, Y. Ipek, S. Marah, I. Demirtas, T. Ozen, DNA protection, molecular docking, antioxidant, antibacterial, enzyme inhibition, and enzyme kinetic studies for parietin, isolated from *Xanthoria parietina* (L.) Th. Fr. J. Biomol. Struct. Dyn. **42**, 848 (2024)
58. M.J. Abraham, T. Murtola, R. Schulz, S. Páll, J.C. Smith, B. Hess, E. Lindahl, GROMACS: high performance molecular simulations through multi-level parallelism from laptops to supercomputers. SoftwareX **1**, 19 (2015)
59. P. Bjelkmar, P. Larsson, M.A. Cuendet, B. Hess, E. Lindahl, Implementation of the CHARMM force field in GROMACS: analysis of protein stability effects from correction maps, virtual interaction sites, and water models. J. Chem. Theory Comput. **6**, 459 (2010)
60. M.S. Valdés-Tresanco, M.E. Valdés-Tresanco, P.A. Valiente, E. Moreno, gmx_MMPBSA: a new tool to perform end-state free energy calculations with GROMACS. J. Chem. Theory Comput. **17**, 6281 (2021)
61. S.S. Gokcimen, T. Ozen, I. Demirtas, S. Marah, F. Gul, L. Behcet, Chemical profile, biological potential, molecular docking, molecular dynamics, and ADMET approaches of essential oils from extracted endemic *Prangos aricakensis* leaf and stem. Fitoterapia **181**, 106391 (2025)
62. S. Yenigun, Y. Basar, Y. Ipek, M. Gok, L. Behcet, T. Ozen, I. Demirtas, A potential DNA protector, enzyme inhibitor and in silico studies of daucosterol isolated from six Nepeta species. Process Biochem. **143**, 234 (2024)
63. M.W. Wong, Vibrational frequency prediction using density functional theory. Chem. Phys. Lett. **256**, 391 (1996)
64. K. Meenakshi, N. Gopal, M. Sarangapani, Synthesis, characterization and antimicrobial activity of some novel Schiff and Mannich bases of isatin. Int J Pharm Pharm Sci **6**, 318 (2014)
65. P. Tarasconi, S. Capacchi, G. Pelosi, M. Cornia, R. Albertini, A. Bonati, P.P. Dall'Aglio, P. Lunghi, S. Pinelli, Synthesis, spectroscopic characterization and biological properties of new natural aldehydes thiosemicarbazones. Biorg. Med. Chem. **8**, 157 (2000)
66. M. Erdoğan, M.S. Çavuş, H. Muğlu, H. Yakan, C. Türkeş, Y. Demir, Ş Beydemir, Synthesis, theoretical, *in silico* and *in vitro* biological evaluation studies of new thiosemicarbazones as enzyme inhibitors. Chem. Biodivers. **20**, e202301063 (2023)
67 I. Fleming, D. Williams, *Spectroscopic Methods in Organic Chemistry*, 7th edn. (Springer, Cham, 2020)
68. H. Muğlu, M.S. Çavuş, T.K. Bakır, H. Yakan, Synthesis of new bis (thiosemicarbazone) derivatives and DFT analysis of antioxidant characteristics in relation to HAT and SET reactions. J. Indian Chem. Soc. **99**, 100789 (2022)
69. H. Yakan, T.K. Bakır, M.S. Çavuş, H. Muğlu, New β-isatin aldehyde-*N*, *N*′-thiocarbohydrazones: preparation, spectroscopic studies and DFT approach to antioxidant characteristics. Res. Chem. Intermed. **46**, 5417 (2020)

70. H. Muğlu, H. Yakan, A.G.A. Misbah, M.S. Çavuş, T.K. Bakır, Synthesis, structure characterization and quantum chemical study on relationship between structure and antioxidant properties of novel Schiff bases bearing (thio)/carbohydrazones. Res. Chem. Intermed. **47**, 4985 (2021)
71. X. Liu, D. Shi, S. Zhou, H. Liu, H. Liu, X. Yao, Molecular dynamics simulations and novel drug discovery. Expert Opin. Drug Discov. **13**, 23 (2018)
72. Y. Başar, S. Yenigün, M.H. Alma, İ Demirtas, T. Ozen, Fruit extracts of *Rosa canina* L. and *Rosa pimpinellifolia* L.: phytochemical profiles, in vitro antioxidant, anti-inflammatory, xanthine oxidase inhibitory effects, and in silico molecular dynamics studies. Kahramanmaraş Sütçü İmam Üniversitesi Tarım ve Doğa Dergisi **28**, 636 (2025)
73. S. Yenigün, Y. Başar, S. Yılmaz, İ Demirtas, T. Ozen, Phytochemical contents and antioxidant activity *Paliurus spina-christi* Miller leaf and seed extracts: PASS predictions, in silico studies on xanthine oxidase and cytochrome P450 1A1. Curr. Perspect. Med. Aromat. Plants **7**, 96 (2024)
74. T. Ozen, M. Demir, S. Marah, H. Korkmaz, In vitro and in silico assessment of bioactivity potencies with components of *Aristolochia bodamae* Dingler extracts from Turkey. ChemistrySelect **9**, e202403703 (2024)
75. S. Cakmak, S. Yenigun, T. Ozen, Preparation, structural analysis, bioactivity assessment, enzyme and molecular docking calculations of some furan/thiophene-2-carboxamide derivatives. J. Iran. Chem. Soc. **20**, 2543 (2023)
76. M. Majewski, S. Ruiz-Carmona, X. Barril, An investigation of structural stability in protein-ligand complexes reveals the balance between order and disorder. Commun. Chem. **2**, 110 (2019)

Authors and Affiliations

Hasan Yakan[1] · Halit Muğlu[2] · Temel Kan Bakır[2] · Semiha Yenigün[3] · Amhimmid Ghayth Amhimmid Misbah[2] · Muhammet Serdar Çavuş[4] · Tevfik Özen[3]

✉ Hasan Yakan
hasany@omu.edu.tr

✉ Tevfik Özen
tevfkoz@omu.edu.tr

Halit Muğlu
hmuglu@kastamonu.edu.tr

Temel Kan Bakır
temelkan@kastamonu.edu.tr

Semiha Yenigün
cocukdr-sem-hay@windowslive.com

Amhimmid Ghayth Amhimmid Misbah
emhemed1985@gmail.com

Muhammet Serdar Çavuş
mserdarcavus@kastamonu.edu.tr

[1] Department of Chemistry Education, Faculty of Education, Ondokuz Mayis University, 55139 Atakum, Samsun, Turkey

[2] Department of Chemistry, Faculty of Art and Science, Kastamonu University, 37150 Kastamonu, Turkey

[3] Department of Chemistry, Faculty of Sciences, Ondokuz Mayis University, 55139 Atakum, Samsun, Turkey

[4] Biomedical Engineering Department, Faculty of Engineering and Architecture, Kastamonu University, 37150 Kastamonu, Turkey